GEOPHYSICS, VOL. 74, NO. 4 (JULY-AUGUST 2009); P. A47–A52, 4 FIGS.
10.1190/1.3131385

# Stressed swelling clay

Arpita Pal Bathija[1], Haiyi Liang[2], Ning Lu[3], Manika Prasad[4], and Michael Lee Batzle[1]

## ABSTRACT

Clay minerals are present in most sedimentary rocks. They find applicability in a wide range of disciplines, such as material, soil, earth, environmental, and biological sciences. Despite their abundance and use, swelling of clays under stress has not received enough scientific attention. We used a two-method approach, consisting of molecular simulation and nanoindentation measurements on montmorillonite. Our analyses of the molecular structure of montmorillonite at various stresses and hydration states showed that swelling behaves in a nonlinear way with stress. Nanoindentation results of Young's modulus agree with our simulation results, showing the importance of the interlayer in composite clay properties.

## INTRODUCTION

Extensive modeling and experimental research show that hydration of swelling clays nonuniformly increases their basal spacing (Mooney et al., 1952; Skipper et al., 1995; Karaborni et al., 1996). However, large regions of the phase space at extreme stress (higher than atmospheric pressure) and at high water content remain relatively unexplored. These extreme conditions can help us understand and model the enhancement of material properties (Zunjarrao et al., 2006) and explore the possibility of life originating in montmorillonite (Ferris, 1993).

Nanoscale measurements for mineral properties of swelling clays such as montmorillonite with quantifiable interlayer water under high stress have not been done before because of their small grain size, the highly reactive behavior of these nanominerals to polar molecules, and a lack of appropriate tools. A molecular simulation approach provides a means to simulate these measurements (Skipper et al., 1995; Chavez-Paez et al., 2001), and nanoindentation is a way to perform those experiments.

## MOLECULAR SIMULATION

We conducted a Monte Carlo-based equilibrium study on sodium-saturated Wyoming-type montmorillonite under high stress and varying water contents. The system setup includes representing molecules as collections of atom-centered interaction sites, using classical force fields for the potential energy terms, and implementing periodic boundary conditions (Allen and Tildesley, 1987; Frenkel and Smit, 2002). A new configuration is generated by selecting a random molecule, translating it, rotating it, and performing internal structural variations. Acceptance of the new configuration is determined by the Metropolis sampling algorithm (Metropolis et al., 1953); application over enough configurations yields properly weighted averages for structure and thermodynamic properties.

An isothermal-isobaric ensemble of a system enabled us to study the equilibrium structures at constant temperatures, pressures, and water content. The simulations were made at discrete uniaxial stresses (1 Pa to 10 GPa) applied normal to the clay sheets with varying numbers of water molecules (0–128) in the interlayer at a constant temperature (300 K). The intermolecular potential energy terms (Skipper et al., 1995) were assumed to be valid and constant for all stress and water content considered in this study. (See Appendix A for details on the simulation method.)

The simulations captured equilibrium basal spacing (thickness of the clay layer and the interlayer) of montmorillonite as a function of stress and bound water in the interlayer with a maximum uncertainty of 1.8%. Our simulated basal spacing at 0.1 MPa and 32 water molecules (12.27 Å) is in close agreement with experimental data (12.2–12.5 Å) (Mooney et al., 1952) and previous simulation data (12.1 Å) (Skipper et al., 1995).

The basal spacing increases with increasing water content (Figure 1). The interlayer expands as the interlayer cations are attracted more to water than to the relatively small negative clay-layer charge (Moore and Reynolds, 1989). At a constant hydration state, the basal spacing decreases with increasing uniaxial stress. The simulated hydration-induced expansion in montmorillonite under stress (Figure 1) exhibits a separation in deformation behavior at about 1 MPa. Be-

Manuscript received by the Editor 24 October 2008; revised manuscript received 24 February 2009; published online 11 June 2009.
[1]Colorado School of Mines, Department of Geophysics, Golden, Colorado, U.S.A. E-mail: abathija@mines.edu; mbatzle@mines.edu.
[2]Harvard University, Division of Applied Science and Engineering, Cambridge, Massachusetts, U.S.A. E-mail: hyliang@seas.harvard.edu.
[3]Colorado School of Mines, Division of Engineering, Golden, Colorado, U.S.A. E-mail: ninglu@mines.edu.
[4]Colorado School of Mines, Petroleum Engineering Department, Golden, Colorado, U.S.A. E-mail: mprasad@mines.edu.

low 1 MPa (domain A), basal spacing changes with stress are on the order of uncertainty in simulation data. Stress can be ignored as a factor in the swelling of clays for shallow depths (~100 m) (Boek et al., 1995).

Between 1 MPa and 10 GPa (domain B), which encompasses deeper burial and the subduction zone, basal spacing shows maximum sensitivity to stress. The effect of stress also increases with higher water content in domain B. The nonlinear trend of basal spacing with stress is similar to the volume changes of water with pressure (Bowers, 1995). The relationship between applied stress and displacement of the interlayer is highly nonlinear, in contrast to the linear behavior in pyrophyllite (Katti et al., 2005b). This difference occurs because of the interaction between the clay layers and the interlayer water and cations, which are absent in uncharged pyrophyllite.

Our study establishes that the swelling behavior of clays under stress cannot be explained by bulk liquid water properties but is an intricate interplay of the siloxane surface, cation solvation effects, and stress on the interlayer water. To investigate the interplay of the clay layers and cations with interlayer water, the simulated partial radial distribution functions (RDFs) of the interlayer water molecules are compared with those of bulk liquid water (Soper et al., 1997). Molecular mechanisms underlying the structural differences can be interpreted from the partial RDFs for hydrogen-oxygen H-O ($g_{HO}(r)$), hydrogen-hydrogen H-H ($g_{HH}(r)$), and oxygen-oxygen O-O ($g_{OO}(r)$) spatial correlations (Sposito et al., 1999) as functions of water content (Figure 2) and stress (Figure 3). Partial RDFs in bulk water indicate the relative placement of water molecules about a reference molecule, with the first peak indicating the nearest neighbor position, the second the position of next nearest neighbors, etc.

The partial RDFs for H-H, O-O, and H-O with increasing water content in the interlayer show better-defined peaks, resembling bulk liquid water (Figure 2). However, the organization of the interlayer water molecules differs significantly from the local tetrahedral coordination characteristic of bulk liquid water. Strong spatial correlations in interlayer water are seen from the appearance of certain peaks. The shifting of certain peaks to larger distances $r$ than in bulk water (indicating longer hydrogen bonds) shows that the spatial correlations extend over greater distances. These structural differences result from the interaction of the clay mineral surface and cation solvation effects in organizing the interlayer water.

The diminishing or weakening of certain peaks (Figure 3) indicates that the organization of the interlayer water molecules is disrupted with increasing uniaxial stresses. Shifting of peaks toward lower $r$ values than the bulk liquid behavior show that the spatial correlations exist over shorter distances, implying shorter hydrogen bonds at higher stresses.

The equilibrium structures under stress give the elastic modulus of the interlayer because the clay layers are kept stiff in the simulation model. The change in basal spacing with stress is used to calculate the compressional modulus. Young's modulus is calculated assuming a constant Poisson's ratio $\nu$ of 0.144 (Woeber et al., 1963). The magnitude of the calculated Young's modulus varies because of Poisson's ratio (16 GPa for $\nu = 0.11$ to 2 GPa for $\nu = 0.48$), but the behavior with water content and stress remains the same. Young's modulus for a sodium (Na) montmorillonite interlayer, normal to the clay sheets ([001] orientation), is between 5 and 16 GPa for varying amounts of water and stress. Thus, the range of Young's modulus from simulations also encompasses the major part of the difference attributable to Poisson's ratio.

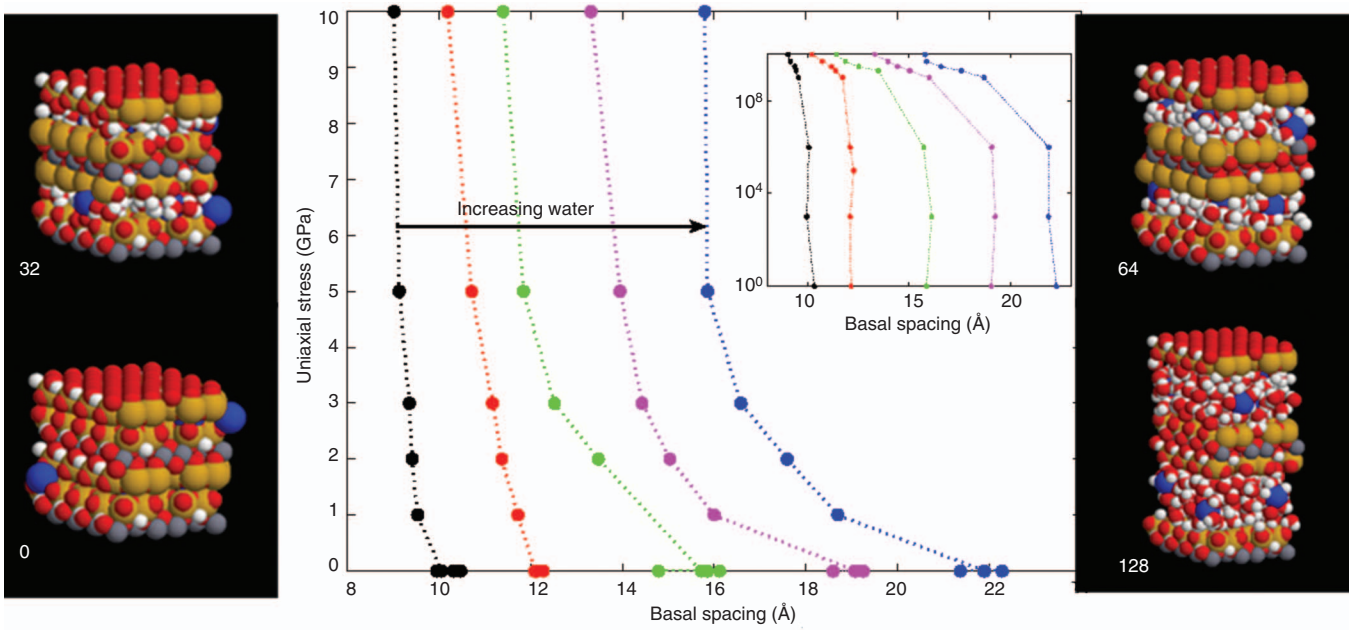


Figure 1. Hydration-induced expansion in montmorillonite under stress. Effects of uniaxial stress, applied normal to the clay sheets, on basal spacing are shown with varying numbers of water molecules in the interlayer. The inset shows the same data with the stress plotted in logarithmic scale. Black represents zero water molecules; red, 32; green, 64; magenta, 96; and blue, 128. Surrounding the plot are the stable-state structures obtained from simulation runs for 0, 32, 64, and 128 water molecules in the interlayer at 1 GPa of uniaxial stress. Gold represents silicon atoms; white, hydrogen; red, oxygen; green, magnesium; blue, sodium; and gray, aluminum. Swelling increases with water content and decreases with uniaxial stress. At a constant hydration state, basal spacing changes are insignificant below 1 MPa; between 1 MPa and 10 GPa, they are affected by stress in a nonlinear way.

Steps occur in the Young's-modulus profile with the start of new water layers, but those steps become smaller and wider with successive water layers. These changes in modulus can be explained by density variations (Music et al., 2003) of the interlayer water. The density variations are related to the arrangement of water molecules in the interlayer (Boek et al., 1995). Our work might help in understanding the feasibility of finding montmorillonite at extreme conditions, an unanswered question in origin-of-life studies (Ferris, 1993).

## NANOINDENTATION

Nanoindentation measurements were performed on two different reference montmorillonites (Wyoming SWy 2 and Otay SCa 3) to compare with our simulation results. Nanoindentation uses a magnetic assembly to load a sharp, diamond nanoindenter device into a sample. This device directly measures the displacement into the sample with a capacitance gauge. The nanoindenter has a continuous stiffness measurement (CSM) option (Oliver and Pharr, 1992) that measures the elastic and plastic responses of the material during loading. The CSM option is especially useful for evaluating thin films on substrates because the mechanical properties change as a function of surface penetration.

The load and stiffness values with indentation depth are measured; these lead to calculations of Young's modulus and hardness. The load curve is monitored for any discontinuities or plasticity (pop-ins) to avoid analyzing data in the plastic regime. The difficulty in making accurate measurements of the contact area during indentation significantly limits the accuracy of data analysis. Dividing load $P$ by the square of the stiffness $S$ results in an expression independent of the contact area and is therefore a material characteristic (Joslin and Oliver, 1990).

The concept that the Young's modulus and hardness values represent the true material properties in the range where the material char-

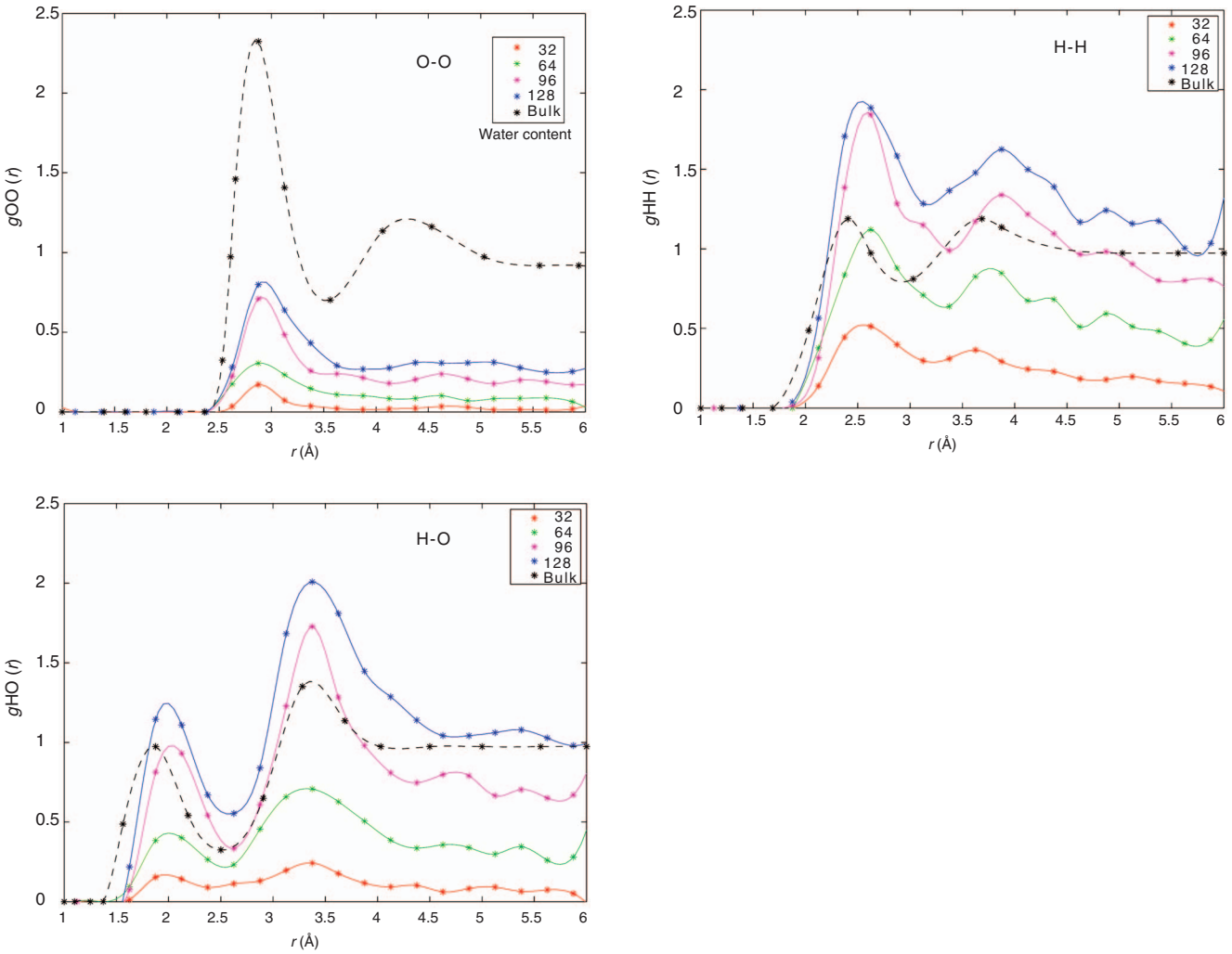


Figure 2. Simulated partial RDFs with varying water content for hydrated Na-montmorillonite (solid lines) and for bulk water from neutron diffraction data (dashed lines) (Soper et al., 1997). All of the partial RDFs correspond to a constant stress of 0.1 MPa. Partial RDFs for montmorillonite with 32, 64, 96, and 128 water molecules in the interlayer are shown for comparison. With increase in water content in the interlayer, the partial RDFs for H-H, O-O, and H-O show better-defined peaks. However, the organization of the interlayer water molecules differs significantly from the local tetrahedral coordination that is characteristic of bulk liquid water. Strong spatial correlations in interlayer water are seen from the appearance of certain peaks. The shifting of some peaks to larger distances $r$ than in bulk water (indicating longer hydrogen bonds) shows the spatial correlations extend over greater distances.

acteristic is constant with indentation depth is based on experiments performed by Saha and Nix (2002) and is used in all our data analyses. Young's modulus of muscovite film on glass substrate is characterized as part of the calibration procedure (61 ± 1 GPa). Our values are comparable to 61 GPa using brillouin scattering measurements (McNeil and Grimsditch, 1993). Appendix A provides details on sample preparation and characterization.

Young's modulus values of 4–14 GPa were obtained for two different types of natural reference montmorillonite (SCa 3 and Swy 2) from nanoindentation; they matched reasonably well with our simulation results (5–16 GPa). The results from one of the measurements for SCa 3 are shown in Figure 4. Nanoindentation gives us the composite of clay and interlayer properties. Molecular simulation gives us the interlayer property alone because the clay layers were kept stiff.

Katti et al. (2005a) study Na-montmorillonite using molecular dynamics and found that most of the deformation occurs in the interlayer. Being the softer component, the interlayer is responsible for most of the deformation and dominates clay mechanical properties. Nanoindentation measurements for Young's modulus could not resolve their small changes because of interlayer water content leading to similar values for SCa 3 and SWy 2, although they had different water content.

The greatest challenge of achieving good contact between the indenter tip and the sample was overcome by taking larger grain sizes, reducing the strain rate, and making the surface of the sample very smooth and free of impurities. Although the samples were pure clay minerals, they had minor amounts of impurities such as quartz and feldspar (Chipera and Bish, 2001).

One of the reasons for variance in our measurement values could be the indenter tip contacting the impurities, although the SWy 2 sample was centrifuged to exclude the larger impurities and each indentation spot was chosen carefully in both samples. A microscope with better resolution linked to the nanoindenter might help guide the indenter tip to avoid the impurities with more certainty. Another reason for the variations in our measurement values could be the

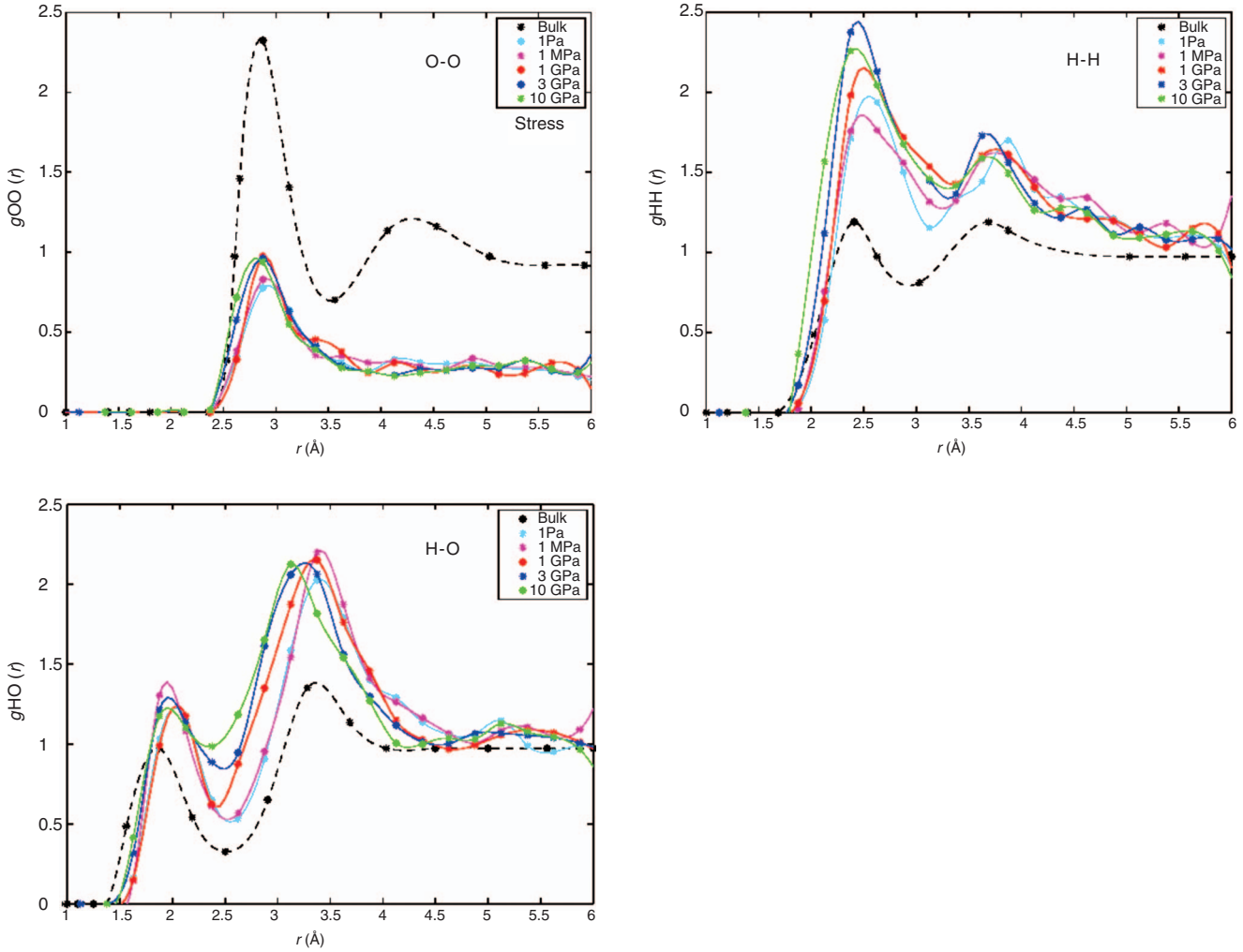


Figure 3. Simulated partial RDFs with varying stress for hydrated Na-montmorillonite (solid lines) and for bulk water from neutron diffraction data (Soper et al., 1997) (dashed lines). Partial RDFs for bulk water correspond to a stress of 0.1 MPa. The partial RDFs for montmorillonite correspond to a constant 128 water molecules in the interlayer and uniaxial stress of 1 Pa, 1 MPa, 1 GPa, 3 GPa, and 10 GPa. The diminishing or weakening of certain peaks indicates the organization of the interlayer water molecules is disrupted with increasing uniaxial stresses. Peaks shifting toward lower *r* values than the bulk liquid behavior show that spatial correlations exist over shorter distances, implying shorter hydrogen bonds at higher stresses.

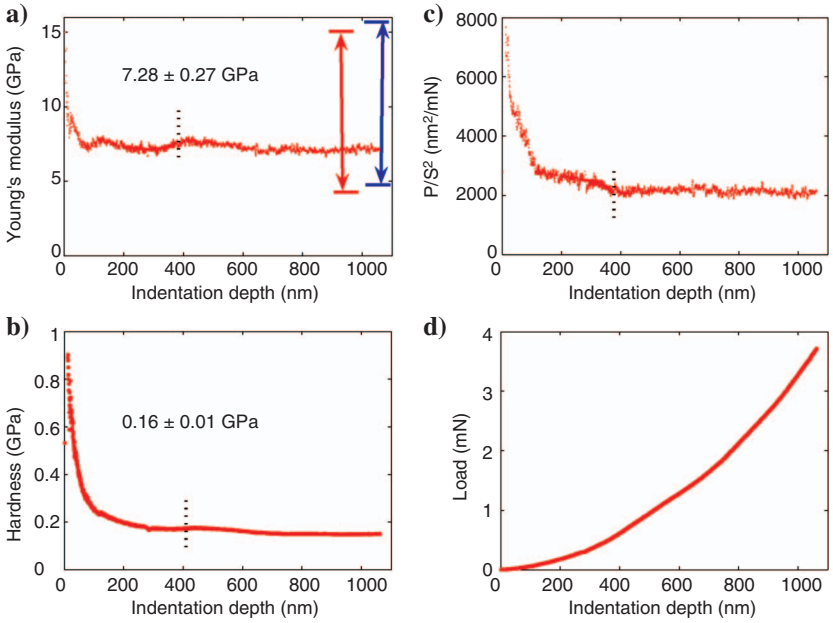


Figure 4. Nanoindentation measurement on montmorillonite (SCa 3) over glass substrate. (a) Young's modulus with indentation depth; (b) material characteristic is constant from 400 nm of indentation depth until the end of data acquisition, shown by dotted line; (c) hardness with indentation depth; and (d) load with indentation depth. Young's modulus of 7.28 ± 0.27 GPa and hardness of 0.16 ± 0.01 GPa were obtained from one of the measurements. The red arrow shows the full range of Young's modulus for montmorillonites obtained from all nanoindentation measurements; the blue arrow shows the same from molecular simulation for montmorillonite.

change in humidity in the environment around the samples during the measurements. Controlled relative humidity measurements might improve data resolution, although the humidity could affect the high-precision nanoindenter adversely.

## CONCLUSIONS

Our analyses of the molecular structure of montmorillonite at various stresses and hydration states show that basal spacing behaves nonlinearly with stress. This study establishes that the swelling behavior of clays under stress cannot be explained by bulk liquid water properties but is an intricate interplay of the siloxane surface, cation solvation effects, and stress on the interlayer water. The changes in modulus can be explained with density variations of the interlayer water, which are related to the arrangement of water molecules.

Nanoindentation gives us the composite of clay and interlayer property properties. Molecular simulation provides the interlayer property alone because the clay layers are kept stiff. Being the softer component, the interlayer is responsible for most of the deformation and dominates the clay mechanical properties. This agreement between independent modeling and experimental approach validates our results but opens up new areas of discussion.

## ACKNOWLEDGMENTS

The authors thank the Petroleum Research Fund (PRF 43596-AC8), the Clay Minerals Society, the Norwegian Research Council (Award 2007/9098-LIGU), and the Fluids Consortium for financial support. We appreciate the help from the reviewers and editors to improve the manuscript. We are grateful to Moneesh Upmanyu and Richard Wendlandt for advice and help. The authors thank Ivar Reimanis and Masood Hashemi for help with the nanoindentation measurements.

## APPENDIX A

## SIMULATION METHOD

A unit cell of the modeled montmorillonite has the following chemical formula:

$$(Si_{7.75}Al_{.25}) \times (Al_{3.50}Mg_{.50})O_{20}(OH)_4Na_{.75}.nH_2O.$$

It has an unbalanced layer charge of $-0.75$, 33% of which is in the tetrahedral sheet. The starting structure has a unit cell measuring $5.28 \times 9.14 \times 6.56$ Å (Skipper et al., 1995). Our simulation model (Katti et al., 2005b) has two clay layers, each containing four unit cells in the $x$-direction and two unit cells in the $y$-direction. There are four magnesium (Mg) ions in the octahedral layer, two aluminum (Al) ions in the tetrahedral layer, and six sodium (Na) ions in the interlayer of each clay layer to balance the layer charge.

The Matsuoka, Clementi, and Yoshimine (MCY) model for the interaction between two water molecules is used (Matsouka et al., 1976). The functional form for potential energy $V(r_{ij})$ (in kilocalories, or kcal) is shown in equation A-1:

$$V(r_{ij}) = -A_{ij}e^{-B_{ij}r_{ij}} + C_{ij}e^{-D_{ij}r_{ij}} + \frac{q_iq_j}{r_{ij}}, \qquad \text{(A-1)}$$

where $A_{ij}$, $B_{ij}$, $C_{ij}$, and $D_{ij}$ describe the interactions between a particular pair of sites $i$ and $j$; $q_i$ and $q_j$ are the effective charges (in coulombs) on a site; and $r_{ij}$ (in angstroms) is the intermolecular site separation. The values $A_{ij}$, $C_{ij}$ (in kcal/mole) and $B_{ij}$, $D_{ij}$ (in Å$^{-1}$) are potential function constants. The first term represents the attractive London or dispersion forces (Van der Waals forces), the second term the short-range repulsions, and the third term the Coulomb force between charged sites.

Various other forms are also used, e.g., the empirical TIP4P (Jorgensen et al., 1983) form, but the MCY model has a considerable advantage in modeling hydrated clay systems (Skipper et al., 1995). The cation-cation interaction is purely ionic and is modeled as a simple pairwise electrostatic interaction (Teppen et al., 1997). The clay interaction parameters (Skipper et al., 1991; Park and Sposito, 2003) are used.

Data were collected for averages after every 5000 attempted moves. The simulations were allowed to proceed until equilibration was reached, which was at least 500,000 moves. Equilibration was judged to have occurred when the average total potential energy of the system and $z$-dimension of the layer (basal spacing) exhibited reasonably constant values.

The partial radial distribution function $g_{\alpha\beta}(r)$ is defined implicitly by (Enderby and Neilson, 1981):

$$dn_{\alpha\beta} = 4\pi \frac{N_\beta}{V} g_{\alpha\beta}(r) r^2 dr, \qquad \text{(A-2)}$$

where $dn_{\alpha\beta}$ is the average number of $\beta$-species atoms within a spherical shell of radius $r$ and thickness $dr$ enclosing an $\alpha$-species atom that has been placed at $r = 0$. The value $N_\beta$ is the total number of $\beta$ atoms in the system of volume $V$. Thus, $g_{\alpha\beta}(r)$ is the relative probability that a $\beta$ atom resides within $dr$ at a radial distance $r$ from an $\alpha$ atom centered at the origin of coordinates (Allen and Tildesley, 1987).

## Sample preparation and characterization

Nanoindentation studies were done on different montmorillonites (SWy 2 and SCa 3) from the Source Clays Repository of the Clay Minerals Society on glass substrate. First, powdered SWy 2 was mixed with distilled water and centrifuged to restrict the grain size. Then it was deposited on glass substrate and left in a covered case for 48 hours to dry. This method forced the clay mineral to align with the *c*-axis normal (in [001] orientation) to the glass slide. A small, smooth piece of SCa 3 (as received) was chosen and glued on glass substrate. The orientation was checked with an environmental scanning electron microscope (ESEM). An ESEM works on low vacuum, so it does not totally dry out the sample—very important for montmorillonites because they always contain water. The precise water content was quantified with thermogravimetric analysis (TGA) for both montmorillonites samples. Sample SWy 2 had 50% water and SCa 3 had 18% water by weight. The muscovite sample was $39.76 \pm 1.75$ μm thick, and the average roughness was 2.25 μm. The montmorillonite (SWy 2) sample was 6 μm thick and the average roughness was 1.36 μm.

## REFERENCES


Allen, M., and D. Tildesley, 1987, Computer simulation of liquids: Oxford University Press.

Boek, E., P. Coveney, and N. Skipper, 1995, Monte Carlo molecular modeling studies of hydrated Li-, Na-, and K-smectites: Understanding the role of potassium as a clay swelling inhibitor: Journal of the American Chemical Society, **117**, no. 50, 12608–12617.

Bowers, T., 1995, Pressure-volume-temperature properties of $H_2O$–$CO_2$ fluids, *in* T. Ahrens, ed., Rock physics and phase relations: A handbook of physical constants: American Geophysical Union.

Chávez-Páez, M., K. Van Workum, L. de Pablo, and J. J. de Pablo, 2001, Monte Carlo simulations of Wyoming sodium montmorillonite hydrates: Journal of Chemical Physics, **114**, no. 3, 1405–1413.

Chipera, S., and D. Bish, 2001, Baseline studies of the Clay Minerals Society source clays: Powder X-ray diffraction analyses: Clays and Clay Minerals, **49**, no. 5, 398–409.

Enderby, J., and G. Neilson, 1981, The structure of electrolyte solutions: Reports on Progress in Physics, **44**, 593–653.

Ferris, D. J. P., 1993, Montmorillonite catalysis of RNA oligomer formation in aqueous solution: A model for the prebiotic formation of RNA: Journal of the American Chemical Society, **155**, no. 11, 12270–12275.

Frenkel, D., and B. Smit, 2002, Understanding molecular simulation: Academic Press Inc.

Jorgensen, W. L., J. Chandrasekhar, J. D. Madura, R. W. Impey, and M. L. Klein, 1983, Comparison of simple potential functions for simulating liquid water: Journal of Chemical Physics, **79**, 926–935.

Joslin, D., and W. Oliver, 1990, A new method for analyzing data from continuous depth-sensing microindentation tests: Journal of Materials Research, **5**, no. 1, 123–126.

Karaborni, S., B. Smit, W. Heidug, J. Urai, and V. E. Oort, 1996, The swelling of clays: Molecular simulations of the hydration of montmorillonite: Science, **271**, 1102–1104.

Katti, D., K. Katti, S. Schmidt, and P. Ghosh, 2005a, An insight into clay-water molecular interactions in the interlayer of Na-montmorillonite subject to external stress: 3rd Biot Conference on Poromechanics, Proceedings, 767–772.

———, 2005b, Modeling the response of pyrophyllite interlayer to applied stress using steered molecular dynamics: Clays and Clay Minerals, **53**, no. 2, 171–178.

Matsouka, O., E. Clementi, and M. Yoshimine, 1976, CI study of the water dimer potential surface: Journal of Chemical Physics, **64**, 1351–1361.

McNeil, L., and M. Grimsditch, 1993, Elastic moduli of muscovite mica: Journal of Physics of Condensed Matter, **5**, 1681–1690.

Metropolis, N., A. Rosenbluth, M. Rosenbluth, and A. Teller, 1953, Equations of state calculations for fast computing machines: Journal of Chemical Physics, **21**, 1087–1092.

Mooney, R., A. Keenan, and L. Wood, 1952, Absorption of water vapour by montmorillonite: Journal of the American Chemical Society, **74**, 1367–1374.

Moore, D. M., and J. R. C. Reynolds, 1989, X-ray diffraction and the identification and analysis of clay minerals: Oxford University Press.

Music, D., U. Kreissig, Z. S. Czigány, U. Helmersson, and J. M. Schneider, 2003, Elastic modulus-density relationship for amorphous boron suboxide thin films: Applied Physics A, **76**, 269–271.

Oliver, W., and G. Pharr, 1992, An improved technique for determining hardness and elastic modulus using load and displacement sensing indentation experiments: Journal of Materials Research, **7**, 1564–1583.

Park, S., and G. Sposito, 2003, Do montmorillonite surfaces promote methane hydrate formation?: Monte Carlo and molecular dynamics simulations: Journal of Physical Chemistry B, **107**, 2281–2290.

Saha, R., and W. Nix, 2002, Effects of the substrate on the determination of thin film mechanical properties by nanoindentation: Acta Materialia, **50**, 23–38.

Skipper, N., F.-R. C. Chang, and G. Sposito, 1995, Monte Carlo simulation of interlayer molecular structure in swelling clay minerals: 1—Methodology: Clays and Clay Minerals, **43**, 285–293.

Skipper, N. T., K. Refson, and J. D. C. McConnell, 1991, Computer simulation of interlayer water in 2:1 clays: Journal of Chemical Physics, **94**, 7434–7446.

Soper, A. K., F. Bruni, and M. A. Ricci, 1997, Site-site pair correlation functions of water from 25 to 400 °C: Revised analysis of new and old diffraction data: Journal of Chemical Physics, **106**, 247–254.

Sposito, G., S.-H. Park, and R. Sutton, 1999, Monte Carlo simulation of the total radial distribution function for interlayer water in sodium and potassium montmorillonites: Clays and Clay Minerals, **47**, 192–200.

Teppen, B. J., K. Rasmussen, P. M. Bertsch, D. M. Miller, and L. Schafer, 1997, Molecular dynamics modeling of clay minerals: 1—Gibbsite, kaolinite, pyrophyllite, and beidellite: Journal of Physical Chemistry B, **101**, 1579–1587.

Woeber, A., S. Katz, and T. Ahrens, 1963, Elasticity of selected rocks and minerals: Geophysics, **28**, 658–663.

Zunjarrao, S., R. Sriraman, and R. Singh, 2006, Effect of processing parameters and clay volume fraction on the mechanical properties of epoxy-clay nanocomposites: Journal of Materials Science, **41**, 2219–2228.